scientific reports

Check for updates

OPEN

[Gly14]-Humanin ameliorates high glucose-induced endothelial senescence via SIRT6

Muqin Li[1,2,3,7], Zhihua Liu[1,7], Xueqin Cao[6,7], Wenjin Xiao[1], Shurong Wang[1], Chengyuan Zhao[1,5], Ying Zhao[4]✉ & Ying Xie[1]✉

High glucose (HG) induced endothelial senescence is related to endothelial dysfunction and cardiovascular complications in diabetic patients. Humanin, a member of mitochondrial derived peptides (MDPs), is thought to contribute to aging-related cardiovascular protection. The goal of the study is to explore the pathogenesis of HG-induced endothelial senescence and potential anti-senescent effects of Humanin. Human umbilical vein endothelial cells (HUVECs) were exposed to glucose to induce senescence, determined by β-galactosidase staining and the expressions of p21, p53, and p16. A clinically relevant dose of HG (15 mM, HG) induced endothelial senescence after 72 h incubation without elevated apoptosis. HG-induced senescence was attributed to the induction of reactive oxygen species (ROS) caused by SIRT6 downregulation, as ROS inhibitor N-acetyl cysteine blocked HG-induced senescence, while inactivation of SIRT6 increased ROS levels and promoted senescence. Strikingly. pretreatment with [Gly14]-Humanin (HNG) antagonized the downregulation of SIRT6 in response to HG and alleviated ROS production and cell senescence. HG-induced reduction of SIRT6 results in ROS overproduction and endothelial senescence. Humanin protects against HG-induced endothelial senescence via SIRT6. This study provides new directions for biological products related to Humanin to be a potential candidate for the prevention of vascular aging in diabetes.

Keywords Humanin, Senescence, SIRT6, Reactive oxygen species, Endothelial cells

Abbreviations

HNG	[Gly14]-Humanin
SIRT6	Sirtuin type-6
MDPs	Mitochondrial-derived peptides
HG	High glucose
ROS	Reactive oxygen species
NAC	N-acetyl cysteine
DM	Diabetes mellitus
CVD	Cardiovascular disease
HUVECs	Human umbilical vein endothelial cells
ECM	Endothelial cell growth medium
ECGS	Endothelial cell growth supplement
FBS	Fetal bovine serum
CCK-8	Cell counting kit-8
PBS	Phosphate buffered saline
PI	Propidium iodide

[1]Department of Endocrinology, The Second Affiliated Hospital of Soochow University, Suzhou 215004, China. [2]Department of Endocrinology, The First People's Hospital of Lianyungang, The Affiliated Lianyungang Hospital of Xuzhou Medical University, The Affiliated Hospital of Kangda College of Nanjing Medical University, Lianyungang 222061, JiangSu, China. [3]Jiangsu Key Laboratory of Neuropsychiatric Diseases and Institute of Neuroscience, Soochow University, Suzhou 215004, China. [4]Department of Pathology and Pathophysiology, School of Basic Medical Sciences, Soochow Medical College of Soochow University, Suzhou 215123, China. [5]Department of endocrinology, Taizhou school of Clinical Medicine, The Affiliated Taizhou People's Hospital of Nanjing Medical University, Nanjing Medical University, 366 Taihu Road, Taizhou 225300, China. [6]Department of Endocrinology, The Fourth Affiliated Hospital of Soochow University, Chongwen Road No. 9, Suzhou 215000, Jiangsu, China. [7]Muqin Li, Zhihua Liu and Xueqin Cao contributed equally to this work. ✉email: yzhao@suda.edu.cn; 13013883877@126.com

Diabetes mellitus (DM) is a group of metabolic diseases characterized by hyperglycemia caused by the direct or indirect deficiency of insulin. Inadequate metabolic management of diabetes can lead to long-term complications, including both macrovascular events and microvascular events[1–3]. In particular, atherosclerotic cardiovascular diseases (CVD) and other macrovascular problems have emerged as the leading causes of mortality in diabetic patients[4–6]. Prevention of cardiovascular complications in diabetic patients has thus received more and more attention.

Various pathological changes in diabetic patients, such as hyperglycemia, hyperlipidemia, and inflammatory stress, played a significant part in the development of atherosclerotic cardiovascular complications[7,8]. Atherosclerotic plaques are initiated by endothelial dysfunction[9,10], a hallmark of numerous cardiovascular diseases[11]. Numerous recent investigations have shown that endothelial dysfunction is partly a consequence of vascular endothelial cell (EC) senescence[12], one of the most dangerous factors in age-related cardiovascular disease[13]. Cell senescence in diabetes could be the direct consequence of high glucose[14,15]and hyperglycemia-induced senescence fuels the development of endothelial dysfunction[16,17]. Thus, it is of utmost importance to impede endothelial senescence in the treatment of vascular complications associated with diabetes mellitus.

In high glucose (HG) conditions, accumulated glycation end products[18], impaired mitochondrial function[19], disordered metabolism[20], etc. can all stimulate cellular stress, thereby promoting the production of cellular reactive oxygen species. The induction of reactive oxygen species (ROS) has been implicated in the induction and maintenance of cell senescence process[21–23]. Of note, the concentration of glucose used in these studies is above 25 mM[24]. This is much higher than the plasma glucose concentration of most diabetic patients that is controlled below 11 mmol/L. More importantly, substantial cell apoptosis is induced by HG at the dose of 30 mM[25] and may interfere with the exploration of the mechanism of HG-induced senescence. Therefore, in the current study, we chose 15 mM HG to more accurately simulate the clinical pathophysiology of HG-induced senescence and figure out a more precise target for clinical treatment.

Humanin, the first member of identified mitochondrial derived peptides (MDPs), plays a cytoprotective role in modulation of mitochondrial function and ROS production under stressful and senescence conditions[26]. More importantly, Humanin is essential for endothelial cells to prevent dysfunction in a mouse model of atherosclerosis[27]. Our previous study proved that 30 mM HG reduces the level of Humanin in human umbilical vein endothelial cells (HUVECs) and pretreating HUVECs with 1μM [Gly14]-Humanin (HNG), a potent analogue) prevents endothelial cell apoptosis via the reduction of ROS[28]. However, whether HNG exerts a protective effect on HG-induced endothelial senescence remains unclear.

In the current study, we explored the pathogenesis of clinically relevant HG-induced endothelial senescence and determined the potential effects of HNG on endothelial protection from senescence. Our data indicates ROS is the key player in the HG-induced endothelial senescence and reduction of ROS contributes to the anti-senescent effect of HNG.

Methods

HUVECs isolation and cell treatment

HUVECs were freshly isolated from individual umbilical cord veins, collected immediately after delivery (39 to 41 weeks), by collagenase digestion[29]. The Second Affiliated Hospital of Soochow University Ethical Committee approved the study, and participants provided informed consent in accordance with the Declaration of Helsinki (JD-LK-2022-095-01).

Primary HUVECs were cultured in Endothelial cell growth media with endothelial growth media Supplement Mix (ScienCell, San Diego, California, USA, cat. no.1001) under standard cell culture conditions (37 °C, 5%CO_2) and used for experiments from passages 6 to 10 until 70–80% confluency. The endothelial growth media contained 5.5mM glucose and supplemented to determined concentration according to different experimental treatments. HG treatment was performed by treating HUVECs with 15 mM or 30 mM glucose for 24 h, 48 h, or 72 h. Controls were performed in the presence of media with normal glucose alone (5.5 mM). High osmotic control was maintained by culturing cells in high mannitol culture media (9.5 mM mannitol plus 5.5 mM glucose or 24.5 mM mannitol plus 5.5 mM glucose). To determine the involvement of reactive oxygen species (ROS) in HG-induced endothelial senescence, HUVECs were treated with or without antioxidant N-acetyl cysteine (NAC) (purity ≥ 99%, Beyotime Biotechnology, Shanghai, China, S0077) at 5 mM. To investigate the effect of SIRT6 on senescence, HUVECs were pretreated with OSS-128,167 (purity ≥ 99%, Selleck Chemicals, Shanghai, China, S8627), a specific SIRT6 inhibitor at 100 μM for 18 h[30]before exposure to HG. To evaluate the anti-senescence effects of HNG (purity ≥ 99%, Sigma, St. Louis, MO, USA, H6161), cells were pretreated with HNG before exposure to HG, Based on our previous research, the treatment of HNG at 1 μM for 3 h is considered as effective treatment time and concentration[28].

Cell counting kit-8 (CCK-8) assay

Cell proliferation was measured by cell counting kit-8 (CCK-8) assay. Cell counting kit-8 (CCK-8) kits were obtained from Med Chem Express (New Jersey, USA, HY-K0301). HUVECs were seeded in 96-well microliter plates at a density of 5×10^3 cells/well, and then treated with high glucose or high osmotic for 72 h with or without pretreatment of HNG. Subsequently, CCK-8 solution was added to each well (1:10 dilution) and then incubated at 37 °C for 2 h. Optical density (OD) was recorded at 450 nm to calculate the relative ratio of cell proliferation. Three independent experiments were conducted to assess the cell proliferation.

Senescence-associated-β-galactosidase activity

SA-β-gal staining was performed according to the manufacturer's instructions. The Senescence β-Galactosidase Staining Kit was purchased from KeyGEN BioTECH (Nanjing, China, KGPAG001). HUVECs were washed

three times in phosphate buffer saline (PBS) (PH 6.0) before being fixed for 30 min in the fixative solution (0.01 M phosphate buffer, 2% formaldehyde, 0.2% glutaraldehyde), washed with PBS (PH 6.0) three times, and then incubated in fresh β-galactosidase staining solution at 37 °C without CO_2 overnight (over 12 h). The number and proportion of SA-β-gal positive cells (more than 50% cyanosis ratio) were counted by randomly selected 5 microscopic fields from each group. Those positive cells were counted by two independent people and three independent experiments were conducted.

Western blot analysis

The total protein of HUVECs was extracted with radio immunoprecipitation assay (RIPA; Beyotime, Shanghai, China, P0013B) solution and the concentration of protein was detected using a BCA kit (ThermoFisher Scientific, Wilmington, DE, USA, 23227). Total protein (30 μg) was loaded in 10% SDS-PAGE and then transferred to a PVDF membrane (Millipore Corporation, Massachusetts, USA, ISEQ00010). The membrane was then blocked with 5% low-fat milk and 0.1% Tween-20 in Tris-buffered saline for 1 h at room temperature for binding non-specific sites. Following, the membrane was cut according to the molecular weight of the target protein and subjected to immunoblotting with corresponding primary antibodies (overnight at 4 °C). After complete washing with 0.1% Tween-20 in Tris-buffered saline (TBST), the membrane was incubated with secondary antibody conjugated with horseradish peroxidase (1:5000, Abcam, Cambridge, England, 97051), and the immunoreactive bands were visualized using an ECL Western Blotting Substrate kit (NCM Biotech, Suzhou, China, P10300). Densitometric analysis of the protein bands was performed using ImageJ software. The relative expression level of target proteins was normalized to the intensity of the β-actin band. Three independent experiments were performed for statistical analysis. Primary antibodies included p21 (1:1000, Invitrogen, Wilmington, DE, USA, 701151), p53 (1:500, Wanleibio, Shenyang, China, WL01919), p16 (1:500, Zenbio, Chengdu, China, R22878), Cyclin D1 (1:1000, Cell Signaling Technology, Boston, USA, 2922 S) and β-actin (1:5000, Sigma, St. Louis, MO, USA, A3854). The protein ladders were purchased from ThermoFisher Scientific (Wilmington, DE, USA, 26616) and Fude biological technology (Hangzhou, China, FD0671).

RNA isolation and real-time quantitative PCR

RNA was isolated from cells using Trizol LS reagent (Invitrogen, Wilmington, DE, USA, 10296010) according to the manufacturer's instructions. RNA quality was measured by Nanodrop spectrophotometer (Thermo Fisher Scientific, Wilmington, DE, USA). cDNA was synthesized from approximately 1000 ng of the RNA for each experiment using a RevertAid™ First Strand cDNA Synthesis Kit (Thermo Fisher Scientific, Wilmington, DE, USA, K16225). The mRNA expression of *18 S*, *SIRT6*, *P53*, *P21*, and *P16* was quantified with SYBR green-based quantitative real-time PCR using a PowerUp™ SYBR™ Green Master Mix (Thermo Fisher Scientific, Wilmington, DE, USA, A25742) on an ABI-7500 (Life Technologies, Darmstadt, Germany) PCR System, and analyzed using the $2^{-\Delta\Delta Ct}$ method. CT values above 35 were defined as undetectable. The mRNA levels of *SIRT6*, *P53*, *P21*, and *P16* were normalized to those of *18 S* to assess the significance of the differences between the groups and three independent experiments were conducted. The primer sequences were as follows: *SIRT6*, forward 5′-TCCCCG ACTTCAGGGGTC-3′, reverse 5′-GTTCTGGCTGACCAGGAAGC-3′; *P53*, forward 5′-CCTCAGCATCTTAT CCGAGTGG-3′ and reverse 5′-TGGATGGTGGTACAGTCAGAGC-3′; *P21*, forward 5′-AGGTGGACCTGGA GACTCTCAG-3′ and reverse 5′-TCCTCTTGGAGAAGATCAGCCG-3′; *P16*, forward 5′-AGGTCATGATGA TGGGCAGC-3′ and reverse 5′-AATCGGGGATGTCTGAGGGA-3′, *Cyclin D1* forward 5′- CTGTGCTGCGA AGTGGAAAC-3′ and reverse 5′- TCTGTTTGTTCTCCTCCGCC-3′, and *18 S*, forward 5′-TCAACACGGGA AACCTCAC-3′ and reverse 5′-CGCTCCACCAACTAAGAAC-3′.

Cell apoptosis assay

The cells were cultured in normal or high glucose conditions for 24 h, 48 h, or 72 h. The percentage of cells undergoing apoptosis was determined by an Annexin V-FITC apoptosis assay kit (YEASEN, Beijing, China, 40302ES60) according to the manufacturer's introductions. The HUVECs were planted in 12-well plates for experimental treatment, and then washed three times with phosphate buffer saline (PBS) and then centrifuged at 800 g for 5 minutes, collecting approximately 3×10^5 cells. Following, the cells were suspended in 500 μL of binding buffer containing 3 μL FITC-conjugated annexin V antibody and 10 μL propidium iodide (PI) and incubated at room temperature for 15 min in the dark. The apoptotic rate of cells was detected by a flow cytometer (BD Biosciences, San Jose, CA, USA) within half an hour, and 3000 cells were measured each time. Propidium Iodide and Annexin V-FITC were mapped in vertical and horizontal coordinates respectively, and the Annexin V positive cells were identified as apoptotic cells. Three independent experiments were conducted.

Measurement of ROS levels

ROS generation was measured by Reactive Oxygen Species Assay Kit (Beyotime Biotechnology, Shanghai, China, S0033s). The HUVECs were harvested and suspended in 500 μL of serum-free medium containing DCFH-DA (1:1000 dilution) and incubated at 37 ℃ for 20 min in the dark. Wash the cells three times with serum-free cell culture medium to fully remove DCFH-DA that has not entered the cells. DCFH fluorescence was detected by the flow cytometer (BD Biosciences, San Jose, CA, USA) and analyzed by Flowjo software (Treestar, Ashland, OR). Three independent experiments were performed for statistical analysis.

Wound healing assay

HUVECs were seeded in 6-well plates at a density of 7×10^5cells/well and cultured in different experimental conditions for different experimental purposes. The scratch was made using a 200 μL pipette tip and washed with phosphate buffer saline three times[31]. Images were taken at the same location using a brightfield inverted microscope at 0, 24, and 36 h after wounding. The furthest distance migrated by the cell monolayer to close

the wounded area during this time period was measured with ImageJ software and calculated by minus 0 h respectively. Results were expressed as a migration index—that is, the migration distance of cells with different treatments relative to that of control cells at the same time point. Experiments were carried out in triplicate and repeated at least three times.

5-Ethynyl-2′-deoxyuridine (EdU) incorporation assay

The cell proliferation of HUVECs was detected by 5-ethynyl-2-deoxyuridine (EdU) incorporation assay. The Cell-LightTM EdU Apollo In Vitro Kit was purchased from Ribobio (Guangzhou, China, C10310-1). After treatment, the HUVECs were incubated and labeled with EdU. After fixation, Apollo staining and Hoechst staining were performed according to the manufacturer's instructions. Subsequently, EdU staining images were obtained with a fluorescence microscope (Olympus, Japan). The results were calculated from three independent experiments.

Transient transfection

HUVECs were seeded in 6-well plates and transfection began when cells had grown to about 50%. The transfection mixture was prepared by mixing serum-free medium, siRNA and Lipofectamine 3000 reagent (Life Technologies, Carlsbad, CA, USA) at a ratio of 50:5:1. 2 ml ECM and 400 ul transfection mixture were added to each cell well and transfection efficiency was determined by western blotting 48 h after transfection. siRNAs for SIRT6 (human) (5′-CCCUGGUCUCCAGCUUAAATT-3′ and 5′-UUUAAGCUGGAGACCAGGGTT-3′) were purchased from GenePharma (Shanghai, China).

Statistical analyses

Results were expressed as mean ± SEM values, and analyzed by GraphPad Prism software (GraphPad Software, La Jolla, CA, USA). Normality and lognormality were assessed with Shapiro-Wilk test using $\alpha = 0.05$, and the assumption of equal variances was analyzed using an F test. For all groups that passed these tests, comparisons between the two experimental groups were determined using two-tailed, unpaired Student's t-test. One-way ANOVA or two-way ANOVA was used for comparisons among multiple groups. A two-tailed *P*-value of less than 0.05 was considered statistically significant.

Results

High glucose induced endothelial senescence via ROS

To explore the effect of HG on cell senescence rather than apoptosis, endothelial cells were treated with different doses of glucose (5.5 mM, 15 mM, and 30 mM) for several time periods (24 h, 48 h, and 72 h). As shown in Fig. 1A, B, the percentage of SA-β-gal positive cells were increased by glucose in a dose- and time-dependent manner. Notably, at a clinically related dose of 15 mM, HG can only induce endothelial senescence instead of apparent apoptosis even after incubation for 72 h (Fig. 1C, D).

In addition to the increase of SA-β-gal positive cells (41.78% vs. 20.26%) (Fig. 2A, B), we also detected significantly increased mRNA levels of p53, p16, p21 for nearly 1.5 times on HUVECs after incubation of HG (15 mM) for 72 h when compared with cells treated with glucose at a dose of 5.5 mM, a normal level in vivo (C) (Fig. 2C–E). The expression of Cyclin D1, a downstream molecule of p21, was reduced by about 40% after HG treatment (Fig. 2F). We verified the protein levels of the above indicators after HG treatment and observed changes consistent with the gene level (Fig. 2G–K). Although the protein levels of p21 only showed a tendency to increase (Fig. 2G, I), HG markedly decreased the expression of Cyclin D1 (~50%) (Fig. 2G, K). In line with the induction of cell senescence, reduced migration, and proliferation of HUVECs were also evident after the treatment with HG (Fig. 2L–P). Given the observations that high mannitol-treated cells did not show any senescence phenotypes and any functional changes, we ruled out the potential contribution of hyperosmolarity to cell senescence (Fig. 2A–P).

In line with previous findings[32,33], we also found that HG increased the cellular levels of reactive oxygen species (ROS) for nearly 2 times in HUVECs (Fig. 3A, B). Considering the potential contribution of ROS in cell senescence[34,35], we employed the N-acetyl cysteine (NAC), an antioxidant precursor to glutathione, to scavenge the excess ROS that increased by HG. As shown in Fig. 3C–K, NAC decreased ratio of SA-β-gal positive cells to levels observed in the control group, indicating the essential role of ROS in HG-induced senescence (Fig. 3C, D). Moreover, a remarkable decrease of p53, p16, and p21 as well as an increase of Cyclin D1 to the levels in the control group were detected in NAC-treated cells in the presence of HG (Fig. 3E–K). Collectively, these results demonstrated that a clinically relevant high dose of glucose can slowly but effectively induce endothelial senescence *via* ROS.

The downregulation of SIRT6 contributes to the induction of ROS in HUVECs by HG

Previous studies have shown that SIRT1 is pivotal regulator in both ROS production and detoxification of endothelial cells[36,37]. However, the expression of SIRT1 was not changed after incubation with glucose at a dose of 15 mM for 72 h (Fig. 4A, B). Strikingly, we detected a marked reduction of SIRT6 at both mRNA and protein levels in HG-treated cells, by about 30% and 50%, while treatment with mannitol at a dose of 15 mM for 72 h did not affect the expression of SIRT6 (Fig. 4A, C, D). Moreover, the elimination of ROS by NAC did not increase the expression of SIRT6 in HG-treated cells (Fig. 4E), implying that the downregulation of SIRT6 by HG was independent of ROS. More importantly, suppression of SIRT6 by its specific inhibitor OSS-128,167 significantly increased the cellular levels of ROS and ROS-associated SA-β-gal positive senescence cells by nearly two times in HUVECs (Figure F-I), indicating the crucial role of SIRT6 in restraining cellular ROS levels and ROS-induced cell senescence. In line with increased SA-β-gal positive senescence cells, inhibition of SIRT6 significantly increased the expressions of p53, p16 and p21 but markedly reduced the expression of Cyclin D1

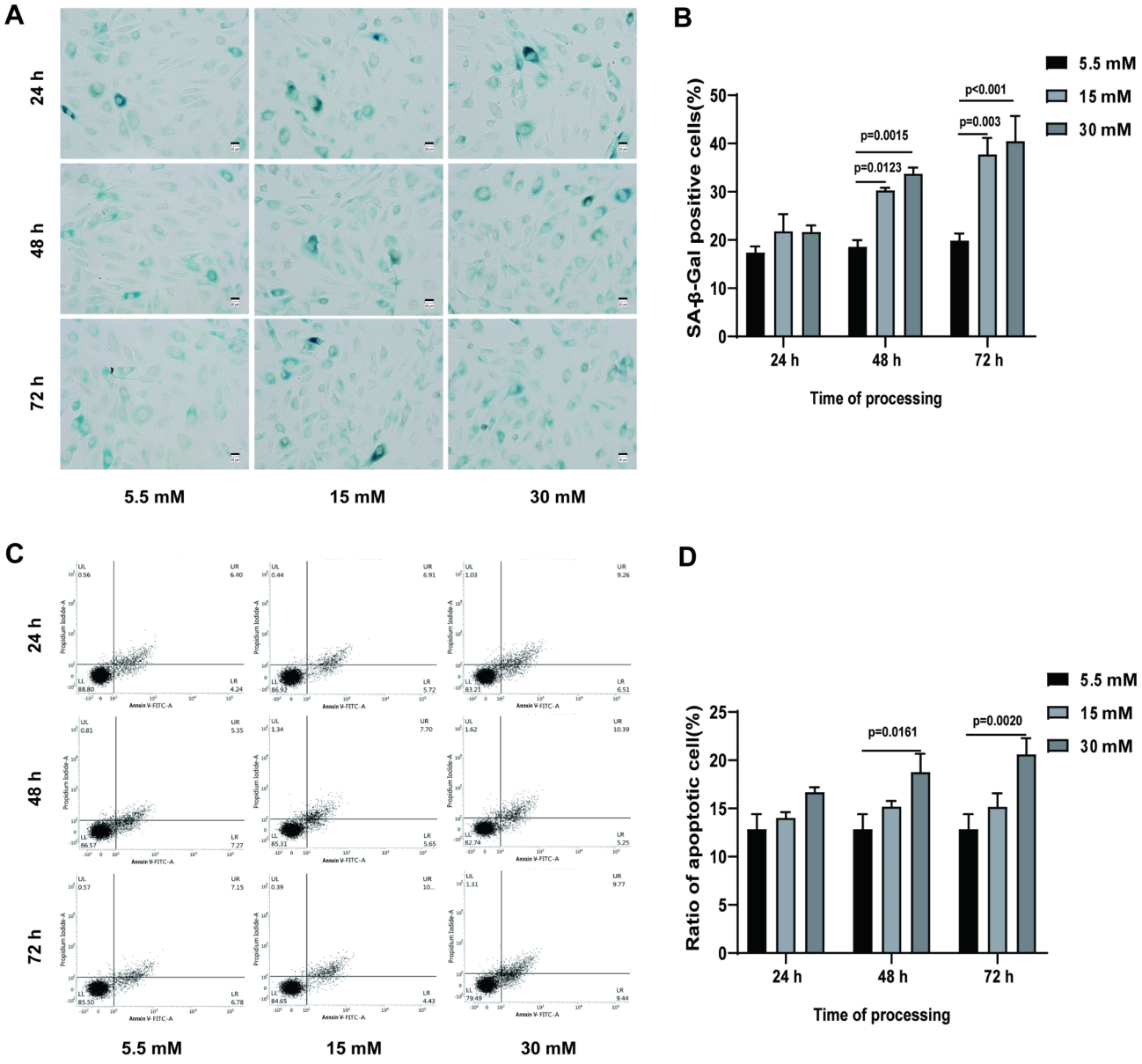

Fig. 1. High glucose induced endothelial senescence in a concentration- and time-dependent manner. (**A**) Representative images of SA-β-gal staining and (**B**) quantification of SA-β-gal positive HUVECs treated with normal glucose (5.5 mM d-glucose), high glucose (15 mM or 30 mM d-glucose) for 24 h,48 h, and 72 h. Scale bar = 20 μm. (**C**) Cell apoptosis assay of HUVECs treated with normal glucose (5.5 mM d-glucose), high glucose (15 mM or 30 mM d-glucose) observed by flow cytometry. (**D**) Analysis of cell apoptosis results of HUVECs. The values are expressed as the mean ± SEM. Experiments were carried out in triplicate and repeated three times. Results in B and D were analyzed with two-way ANOVA with Tukey's multiple comparisons test.

to levels observed in the HG group (Fig. 4J–P). By contrast, pretreatment with OSS-128,167 did not further elevated the cellular levels of ROS and ROS-associated cell senescence in HG-treated cells (Fig. 4F–I). Also, the protein levels of p53, p21, and Cyclin D1 in HG-treated cells were not affected by OSS-128,167 (Fig. 4J-L), although mRNA levels of these molecules were significantly induced (Fig. 4M–P). These data indicated that the reduction of SIRT6 by HG may contribute to ROS-induced cell senescence.

Humanin prevented HG-induced ROS and cell senescence by SIRT6

Next, we tested the effects of Humanin, a member of mitochondrial derived peptides (MDPs), on HG-induced cell senescence. As shown in Fig. 5, the increase of ROS and SA-β-gal positive senescence cells in HG-treated HUVECs were significantly reduced by pretreatment with HNG (Fig. 5A–D). Moreover, HNG regulated the levels of p53, p16, p21 and Cyclin D1 to that observed in the C group (Fig. 5E–G, I–L). These all reflected that

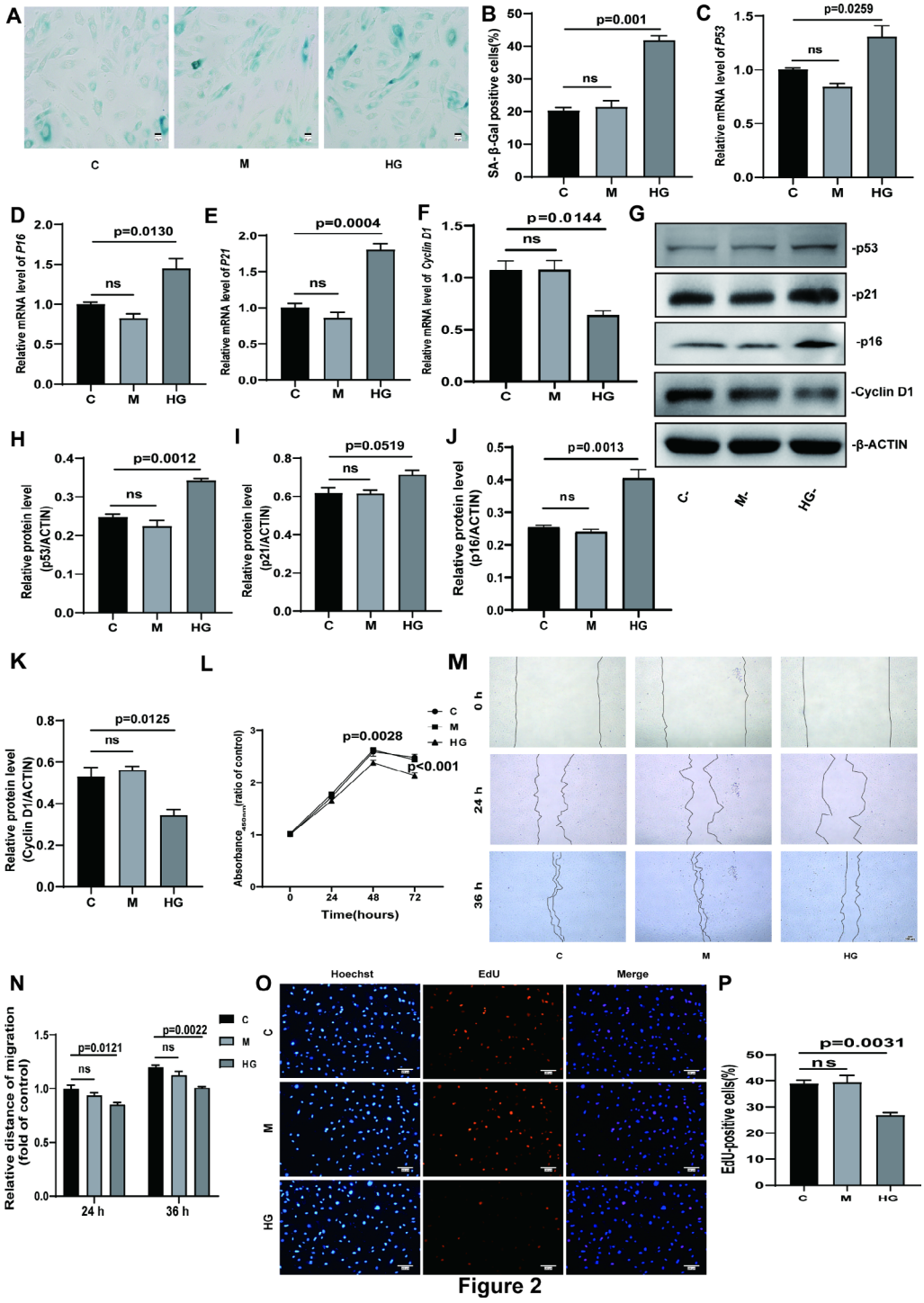

Figure 2

Fig. 2. High glucose led to cell senescence and endothelial cell dysfunction. (**A**) Representative images of SA-β-gal staining and (**B**) quantification of SA-β-gal positive HUVECs treated with normal glucose (5.5 mM d-glucose, C), high mannitol (15 mM mannitol, M), high glucose (15 mM d-glucose, HG). Scale bar = 20 μm. (**C**–**F**) The mRNA levels of (**C**) *P53*, (**D**) *P16*, (**E**) *P21*, and (**F**) *Cyclin D1* of C, M, and HG groups measured by qRT-PCR. (**G**) Representative images of Western Blotting analysis and (H-K) semi-quantification of (**H**) p53, (**I**) p21, (**J**) p16, and (**K**) Cyclin D1 of C, M, HG groups. (**L**) Cell proliferation of C, M, HG groups assessed by CCK-8 assays. Optical density (OD) = 450 nm. (**M**) The representative images of wound healing assay of HUVECs. Scale bar = 100 μm. (**N**) The semi-quantitative analysis of the distance of migration. (**O**, **P**) Representative micrographs of EdU staining (**O**) and quantification (**P**) of EdU positive HUVECs. Scale bar = 100 μm. The values are expressed as the mean ± SEM. Experiments were carried out in triplicate and repeated at least three times. Results in B-F, H-K and P were analyzed with one-way ANOVA with Dunnett's multiple comparisons test. Results in L and N were analyzed with two-way ANOVA with Dunnett's multiple comparisons test.

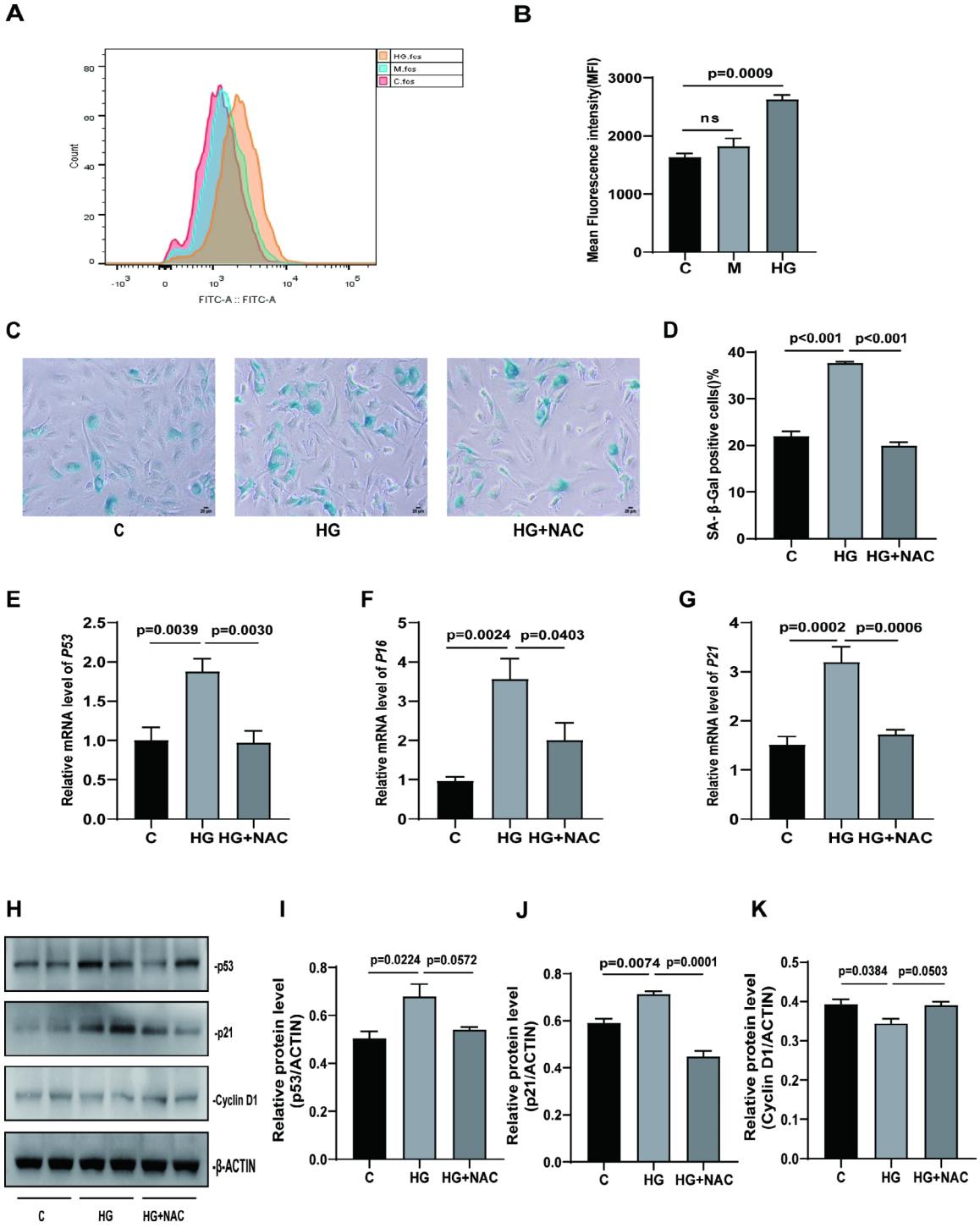

Fig. 3. High glucose induced ROS overproduction and thereby resulted in endothelial senescence. (**A**) ROS levels of HUVECs treated with normal glucose (5.5 mM d-glucose, C), high mannitol (15 mM mannitol, M), high glucose (15 mM d-glucose, HG) detected by flow cytometry. (**B**) Quantitative analysis of DCFH-DA fluorescence intensity in C, M, HG group. (**C**) Representative images of SA-β-gal staining and (**D**) quantification of SA-β-gal positive HUVECs treated with normal glucose (5.5 mM d-glucose, C), high glucose (15 mM d-glucose, HG), high glucose with N-acetyl cysteine (15 mM d-glucose with 5 mM HNG, HG). Scale bar = 20 μm. (**E**–**G**) The mRNA levels of (**E**) *P53*, (**F**) *P16*, and (**G**) *P21* of C, HG HG + NAC groups measured by qRT-PCR. (**H**) Representative images of Western Blotting analysis and (**I**-**K**) semi-quantification of (**I**) p53, (**J**) p21 and (**K**) Cyclin D1 of C, HG HG + NAC groups. The values are expressed as the mean ± SEM. Experiments were carried out in triplicate and repeated three times. Results in B and D were analyzed with one-way ANOVA with Tukey's multiple comparisons test. Results in E were analyzed with one-way ANOVA with Sidak's multiple comparisons test. Results in (**F**, **G**) and (**I**, **K**) were analyzed with one-way ANOVA with Dunnett's multiple comparisons test.

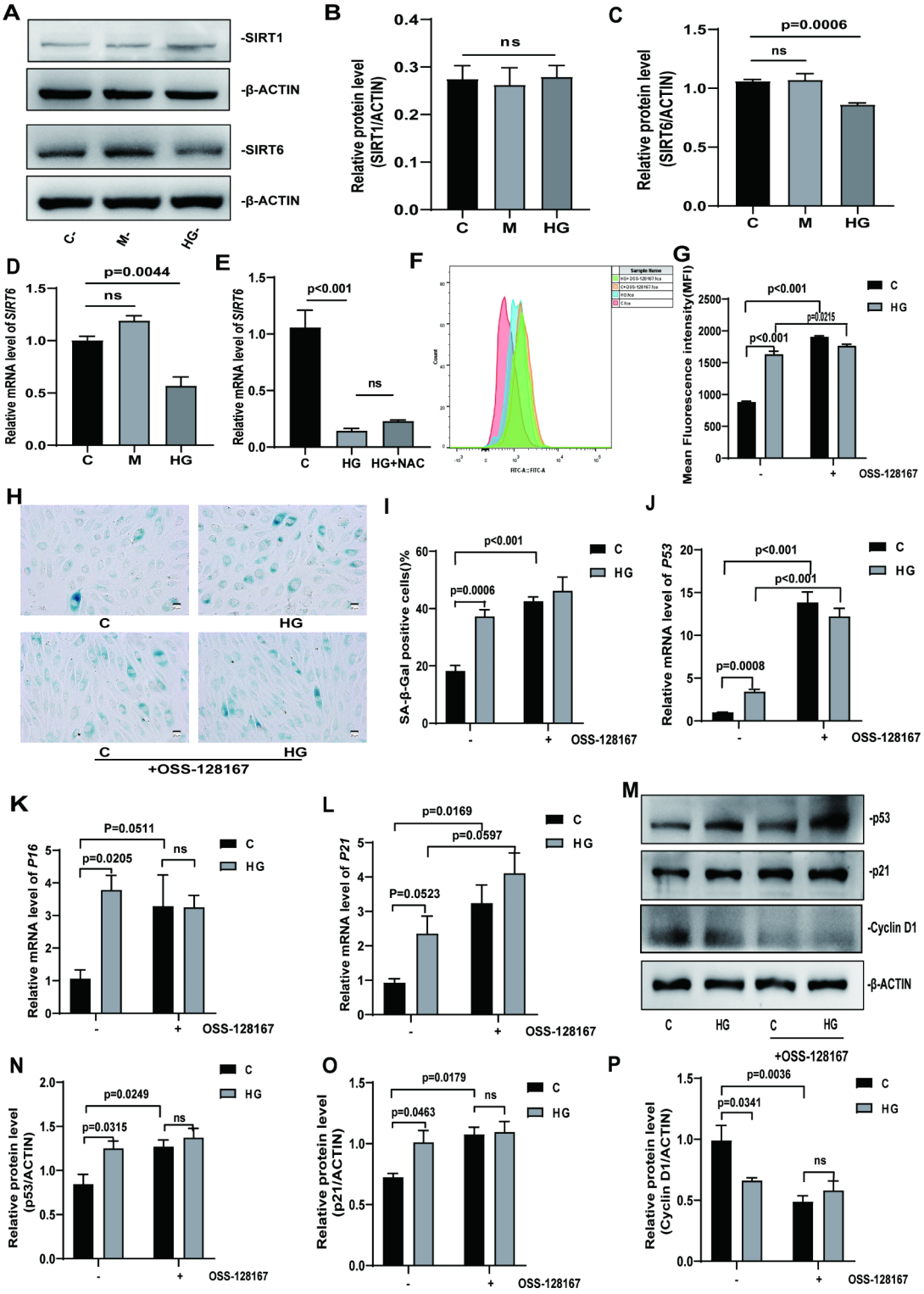

HNG could prevent HG-induced senescence via suppression of ROS. In addition, the anti-senescence effect of HNG was also evidenced as improved cell migration and proliferation as compared to HG-treated HUVECs (Fig. 5O–S).

To further figure out how HNG inhibited the increase of ROS by HG, we checked the effects of HNG on expressions of both SIRT1 and SIRT6. As shown in Fig. 5H, I, M, N, only the reduction of SIRT6 expression by HG was reversed by pretreatment of HNG, which suggests that SIRT6 may have a potential regulatory effect on HNG's rescue of HG-induced ROS overexpression. The pretreatment of OSS-128,167 abolishes the protective effect of HNG against HG-induced senescence. As the result shows (Fig. 6A–I), HNG no longer has the effect of inhibiting the proportion of SA-β-gal positive cells, down-regulating p53, p21, p16 and up-regulating Cyclin D1. HNG also lost its protective impact on cell migration function (Fig. 6J, K) and cell proliferation (Fig. 6L, M) after

◀**Fig. 4**. High glucose downregulated the expression of SIRT6 to increase ROS production and endothelial senescence. (**A**) Representative images of Western blotting analysis and (**B**, **C**) semi-quantification of SIRT6 and SIRT1 in HUVECs treated with normal glucose (5.5 mM d-glucose, C), high mannitol (15 mM mannitol, M), high glucose (15 mM d-glucose, HG). (**D**, **E**) The mRNA levels of *SIRT6* in HUVECs of C, M, HG, HG + NAC groups. (**F**) ROS detection of HUVECs treated with normal glucose (5.5 mM d-glucose, C), high glucose (15 mM d-glucose, HG), normal glucose with OSS-128,167 (5.5 mM d-glucose with 100 μM OSS-128167, C + OSS-128167), high glucose with OSS-128,167 (15 mM d-glucose with 100 μM OSS-128167, HG + OSS-128167) detected by flow cytometry. (**G**) Quantitative analysis of DCFH-DA fluorescence intensity in the four groups. (**H**) Representative images of SA-β-gal staining and (**I**) quantification of SA-β-gal positive HUVECs in the four groups. Scale bar = 20 μm. (**J**–**L**) The mRNA levels of (**J**) *P53*, (**K**) *P16*, (**L**) *P21* of the four groups measured by qRT-PCR. (**M**) Representative images of Western Blotting analysis and (**N**–**P**) semi-quantification of (**N**) p53, (**O**) p21 and (**P**) Cyclin D1 of the four groups. The values are expressed as the mean ± SEM. Experiments were carried out in triplicate and repeated at least three times. Results in B-E were analyzed with one-way ANOVA with Dunnett's multiple comparisons test. Results in G, I-L and N-P were analyzed with two-way ANOVA with Sidak's multiple comparisons test.

suppressing SIRT6. Taken together, all of these findings suggested that HNG's ability to enhance SIRT6 levels in HG is crucial to the anti-senescence mechanism.

To furtherly investigate whether HNG's ability to ameliorate HG-induced senescence depends on SIRT6, we used siRNA to knock down SIRT6. The protein level of SIRT6 significantly decreased by nearly 60% in cells after transfection with SIRT6 siRNA (Fig. 7A, B). Similar to SIRT6 inhibitors, SIRT6 knockdown siRNA abolished the protective effects of HNG on the ratio of senescence HUVECs (Fig. 7C, D) and expression of SIRT6 and senescence related markers (Fig. 7E-J, K-N). Also, the protective effects of HNG on cell migration function (Fig. 7O, P) and cell proliferation (Fig. 7Q, R) were abolished by SIRT6 siRNA. These results furtherly indicated that SIRT6 is essential for HNG's amelioration of HG-induced senescence in HUVECs.

Collectively, these data suggested that Humanin played a protective role against HG-induced endothelial senescence, and this is dependent on its regulation of SIRT6-ROS levels.

Discussion

In the present study, we for the first time to demonstrate that 15 mM of HG effectively induced senescence of the HUVECs without apparent apoptosis after 72 h incubation in vitro. Suppression of SIRT6 by HG stimulates ROS overproduction and promotes endothelial senescence, while pretreatment of HNG can protect HUVECs against HG-induced senescence.

Furthermore, in our clinical practice, it was observed that the control situation of diabetes patients is quite impressive. According to recent epidemiological research, China's diabetes control rate rose to 50.1% in recent years, which means that the hemoglobin A1c (HbA1c) of more than half of diabetes individuals can be kept below 7% (53 mmol/mol)[38]. HbA1c is the predominant fraction of glycosylated hemoglobin and indicates a person's three-month average blood sugar levels. According to the linear regression between HbA1c and mean blood sugar[39], we can learn that the blood sugar of most diabetic patients can be controlled below 11 mmol/L. These statistics show that the majority of patients have relatively low levels of blood sugar control and that only a small subset of patients have extraordinarily high blood sugar levels for an extended period of time. Hence, the lower 15 mM HG was chosen as a clinically relevant dose of high glucose, to more accurately simulate the clinical pathophysiology of HG-induced senescence and provide a more precise target for clinical treatment.

Previous studies have demonstrated glucose metabolism and ROS have reciprocal regulation, HG promoted the generation of ROS in mitochondria, while treatment with the ROS inducer H_2O_2exhibits markedly increased glucose uptake and lipid accumulation[40]. Preview studies showed that HG at dose of above 25 mM stimulated the production of ROS and induced the cell senescence[14,41]. In contrast, our data also demonstrated that clinically relevant lower levels of HG also promote the generation of ROS, a key driver of endothelial senescence. However, mechanisms underlying HG-induced ROS may be different and determined by glucose concentrations and cell types. Related studies have also shown that HG can inhibit the levels of multiple members of the sirtuins family and thus participate in the ROS overproduction[42,43]. Chi Chen et al. 's research on vascular aging shows that exercise promoted skeletal muscle to release FNDC5/irisin-enriched extracellular vesicles and improved the stability of SIRT6, thus delaying vascular aging[44]. The inhibition of SIRT1 is observed by higher doses of HG in human corneal epithelial cells[45], while SIRT6 is suppressed by relatively lower dose of HG in our model. Interestingly, multiple studies have shown the negative relationships of SIRT6 with diabetes[46], whose glucose levels are more close to our study system. More importantly, we found inactivation of SIRT6 by its specific inhibitor OSS-128167 significantly increased ROS production and endothelial senescence.

Mechanisms underlying the downregulation of SIRT6 by clinically relevant HG is still unclear, but our results ruled out the effects of ROS on the expression of SIRT6. Therefore, inhibition of SIRT6 is a cause rather than a consequence of ROS overproduction. Several studies have confirmed the regulatory role of SIRT6 in aging and metabolic related diseases[47,48]. In this study, we found that HG decreased the expressions of SIRT6 while promoted ROS overexpression and cell senescence, all of which can be reversed by pretreatment of HNG. Our data thus indicate that overexpression of SIRT6 may rescue HG-induced cell senescence, which still needs further verification. In addition, the pathway through which HG regulates SIRT6 expression is still unclear. A recent study demonstrated HG regulates the methylation levels of the SIRT6 promoter region, thereby influencing the transcription of SIRT6 in human aortic endothelial cells[49]. Moran Choe and his team found that the RUNX2 transcription factor inhibits the expression of SIRT6 and thus affects cellular glucose metabolism[50].

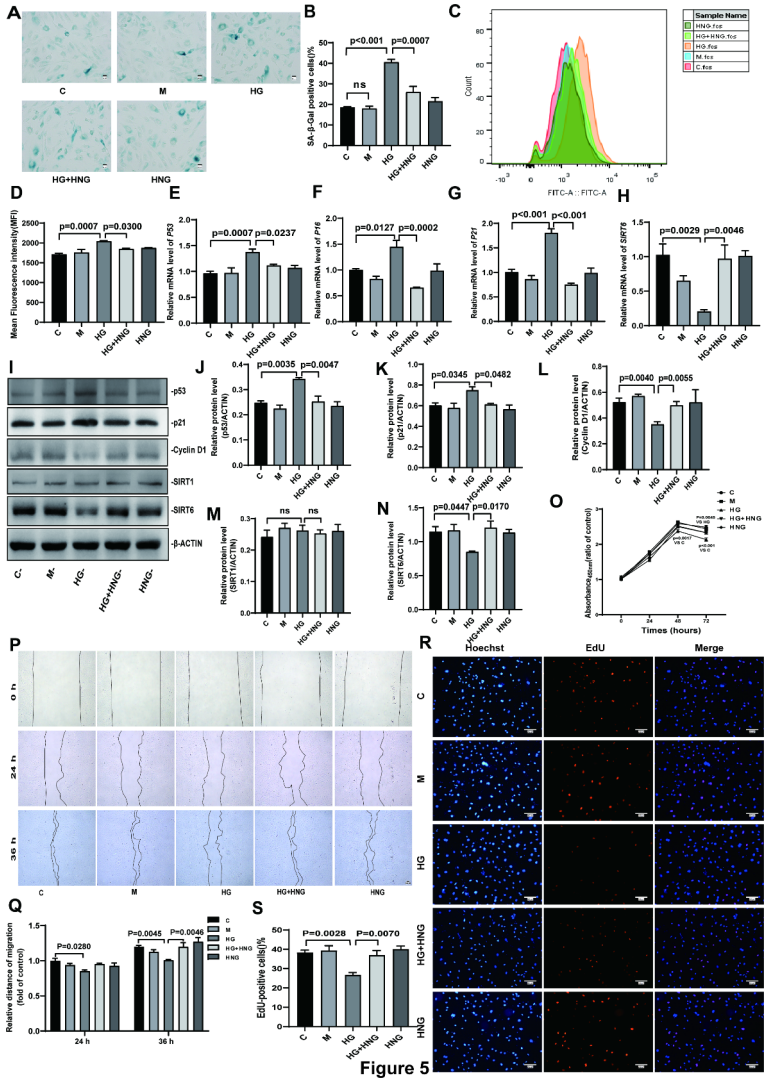

Fig. 5. Humanin prevents HG-induced senescence. (**A**) Representative images of SA-β-gal staining and (**B**) quantification of SA-β-gal positive HUVECs treated with normal glucose (5.5 mM d-glucose, C), high mannitol (15 mM mannitol, M), high glucose (15 mM d-glucose, HG), high glucose with [Gly14]-Humanin (15 mM d-glucose with 1 μM [Gly14]-Humanin, HG + HNG), [Gly14]-Humanin (1 μM [Gly14]-Humanin, HNG). Scale bar = 20 μm. (**C**) ROS detection of HUVECs treated with C, M, HG, HG + HNG, HNG. (**D**) Quantitative analysis of DCFH-DA fluorescence intensity in the C, M, HG, HG + HNG, HNG group. (**E**–**H**) The mRNA levels of (**E**) *P53*, (**F**) *P16*, (**G**) *P21*, (**H**) *SIRT6* of the five groups measured by qRT-PCR. (**I**) Representative images of Western Blotting analysis and (**J**-**N**) semi-quantification of (**J**) p53, (**K**) p21, (**L**) Cyclin D1, (**M**) SIRT1 and (**N**) SIRT6 of the five groups. (**O**) Cell proliferation of C, M, HG, HG + HNG, HNG groups assessed by CCK-8 assays. Optical density (OD) = 450 nm. (**P**) The representative images of wound healing assay of HUVECs of the five groups. (**Q**) The semi-quantitative analysis of the distance of migration. Scale bar = 100 μm. (**R**, **S**) Representative micrographs of EdU staining (**R**) and quantification (**S**) of EdU positive HUVECs. Scale bar = 100 μm. The values are expressed as the mean ± SEM. Experiments were carried out in triplicate and repeated three times. Results in B and D were analyzed with one-way ANOVA with Tukey's multiple comparisons test. Results in E-H, J-N and S were analyzed with one-way ANOVA with Dunnett's multiple comparisons test. Results in Q were analyzed with two-way ANOVA with Dunnett's multiple comparisons test.

Other studies also found that FOXO3a and circRNA circ-ITCH can regulate the level of SIRT6 through different pathways[51,52]. Whether clinically relevant HG regulates the level of SIRT6 through the above pathways warrants further investigation.

In recent years, the potential therapeutic effect of Humanin in neurodegenerative diseases[53], cardiovascular diseases[54], diabetes mellitus[55], and other age-related diseases has also received increasing attention. Multiple experiments have confirmed the effect of Humanin and its potent analogue HNG on increasing lifespan[56], improving insulin resistance[57], and ameliorating hyperglycemia-associated endothelial dysfunction[16]. Our previous study also showed HNG protects HUVECs against relatively higher dose of HG induced apoptosis[28,58].

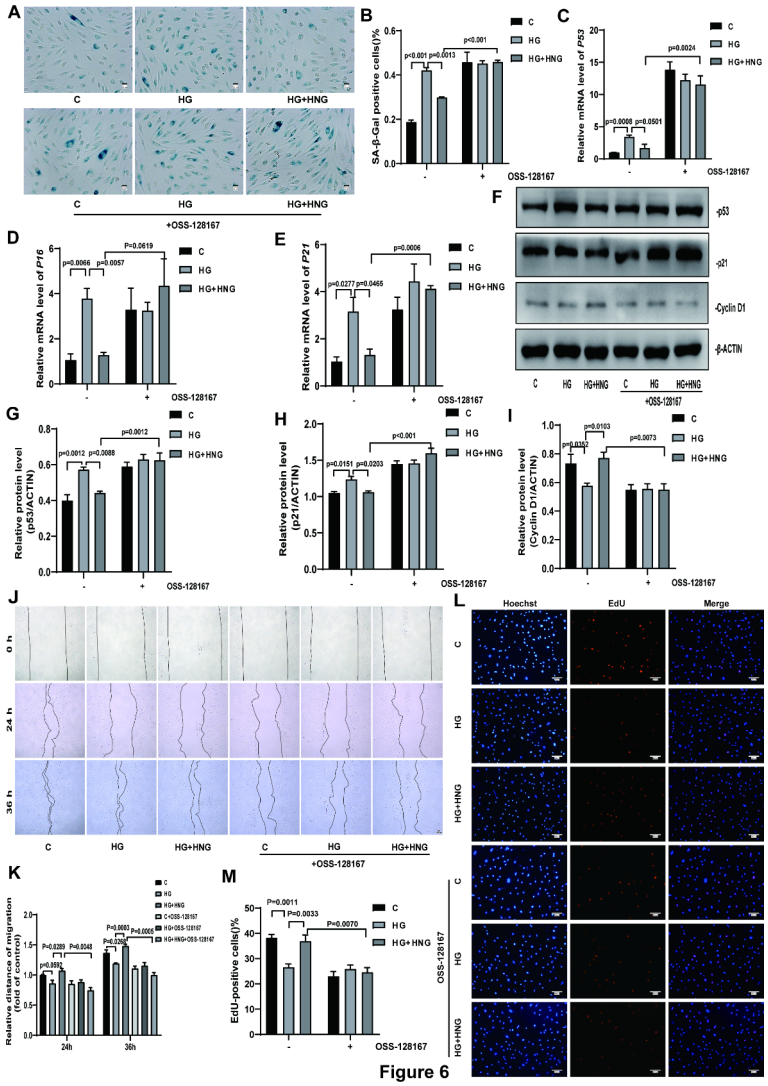

Figure 6

Fig. 6. SIRT6 is required for humanin to protect against HG-induced endothelial senescence. (**A**) Representative images of SA-β-gal staining and (**B**) quantification of SA-β-gal positive HUVECs treated with normal glucose (5.5 mM d-glucose, C), high glucose (15 mM d-glucose, HG), high glucose with [Gly14]-Humanin (15 mM d-glucose with 1 μM [Gly14]-Humanin, HG + HNG), normal glucose with OSS-128,167(5.5 mM d-glucose with 100 μM OSS-128167, C + OSS-128167), high glucose with OSS-128,167(15 mM d-glucose with 100 μM OSS-128167, HG + OSS-128167), high glucose with [Gly14]-Humanin with OSS-128,167 (15 mM d-glucose with 1 μM [Gly14]-Humanin with 100 μM OSS-128167, HG + HNG + OSS-128167). Scale bar = 20 μm. (**C**–**E**) The mRNA levels of (**C**) *P53*, (**D**) *P16*, (**E**) *P21* of the six groups measured by qRT-PCR. (**F**) Representative images of Western Blotting analysis and (**G**-**I**) semi-quantification of (**G**) p53, (**H**) p21, and (**I**) Cyclin D1 of the six groups. (**J**) The representative images of wound healing assay of HUVECs of the six groups. (**K**) The semi-quantitative analysis of the distance of migration. Scale bar = 100 μm. (**L**, **M**) Representative micrographs of EdU staining (**L**) and quantification (**M**) of EdU positive HUVECs. Scale bar = 100 μm. The values are expressed as the mean ± SEM. Experiments were carried out in triplicate and repeated three times. Results in B were analyzed with two-way ANOVA with Sidak's multiple comparisons test. Results in C-E and K were analyzed with unpaired t test. Results in G-I and M were analyzed with two-way ANOVA with Dunnett's multiple comparisons test.

Here, we for the first time demonstrated the anti-senescent effects of HNG on HG-treated HUVECs, partly due to the preservation of SIRT 6 expressions. Interestingly, humanin preserved the expressions of SIRT1 in bone marrow-derived macrophages (BMDMs) isolated from a mouse model of gout[59], indicating that different sirtuins may be involved in its therapeutic effects on different pathological conditions. In other words, the regulation of humanin on the sirtuins family may be an important mechanism for its protective effect, which also indicates its clinical application potential.

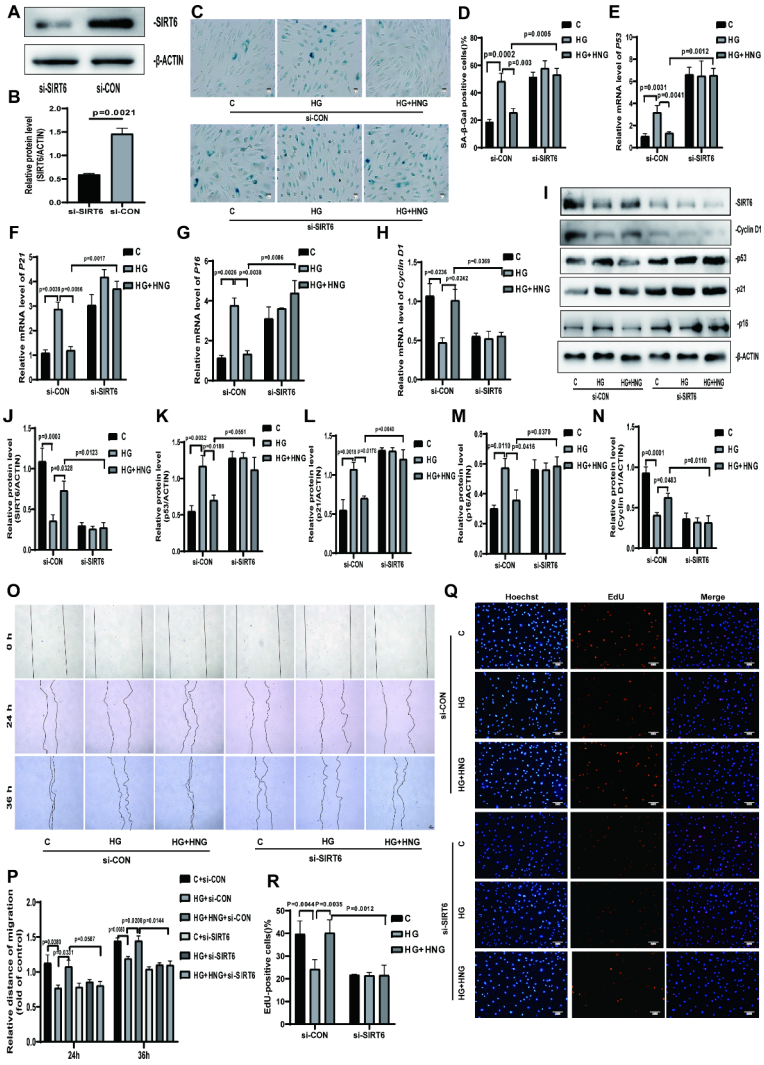

Fig. 7. Knock down of SIRT6 abolished HNG's protection on HG-induced endothelial senescence. (**A**) Western Blotting analysis (**B**) semi-quantification of SIRT6 in HUVECs transfected with SIRT6 or nontargeting siRNA. (**C**) Representative images of SA-β-gal staining and (**D**) quantification of SA-β-gal positive HUVECs treated with normal glucose (5.5 mM d-glucose, C), high glucose (15 mM d-glucose, HG), high glucose with [Gly14]-Humanin (15 mM d-glucose with 1 μM [Gly14]-Humanin, HG + HNG), including transfected with SIRT6 or nontargeting siRNA. Scale bar = 20 μm. (**E**–**H**) The mRNA levels of (**E**) *P53*, (**F**) *P21* (**G**) *P16*, and (**H**) *Cyclin D1* of the six groups measured by qRT-PCR. (I) Representative images of Western Blotting analysis and (**J**-**N**) semi-quantification of (**J**) SIRT6, (**K**) p53, (**L**) p21, (**M**) p16, and (**N**) Cyclin D1 of the six groups. (**O**) The representative images of wound healing assay of HUVECs of the six groups. (**P**) The semi-quantitative analysis of the distance of migration. Scale bar = 100 μm. (**Q**, **R**) Representative micrographs of EdU staining (**Q**) and quantification of EdU positive HUVECs. Scale bar = 100 μm. The values are expressed as the mean ± SEM. Experiments were carried out in triplicate and repeated three times. Results in B, E-H and P were analyzed with Student's t-test. Results in D were analyzed with two-way ANOVA with Sidak's multiple comparisons test. Results in J-N and R were analyzed with two-way ANOVA with Dunnett's multiple comparisons test.

Conclusion

In summary, our results confirm that the regulation of SIRT6 on ROS generation is an important mechanism of HG-induced endothelial senescence, and HNG alleviates endothelial senescence via SIRT6.

Data availability

The data used to support the findings of this study are available from the corresponding author upon request.

Received: 2 June 2024; Accepted: 29 November 2024
Published online: 28 December 2024

References

1. Syed, F. Z. Type 1 diabetes mellitus. *Ann. Intern. Med.* **175**, ITC33–ITC48 (2022).
2. Cole, J. B. & Florez, J. C. Genetics of diabetes mellitus and diabetes complications. *Nat. Rev. Nephrol.* **16**, 377–390 (2020).
3. Forbes, J. M. & Cooper, M. E. Mechanisms of diabetic complications. *Physiol. Rev.* **93**, 137–188 (2013).
4. Katakami, N. Mechanism of development of atherosclerosis and cardiovascular disease in diabetes mellitus. *J. Atheroscler Thromb.* **25**, 27–39 (2018).
5. Kobiyama, K., Ley, K. & Atherosclerosis A chronic inflammatory disease with an autoimmune component. *Circ. Res.* **123**, 1118–1120 (2018).
6. Lehrke, M. & Marx, N. Diabetes mellitus and heart failure. *Am. J. Med.* **130**, S40–S50 (2017).
7. Kane, J. P., Pullinger, C. R., Goldfine, I. D. & Malloy, M. J. Dyslipidemia and diabetes mellitus: Role of lipoprotein species and interrelated pathways of lipid metabolism in diabetes mellitus. *Curr. Opin. Pharmacol.* **61**, 21–27 (2021).
8. Ye, J. et al. Diabetes Mellitus promotes the development of atherosclerosis: the role of NLRP3. *Front. Immunol.* **13**, 900254 (2022).
9. Poznyak, A. et al. The diabetes mellitus-atherosclerosis connection: The role of lipid and glucose metabolism and chronic inflammation. *Int. J. Mol. Sci.* **21**, E1835 (2020).
10. La Sala, L., Prattichizzo, F. & Ceriello, A. The link between diabetes and atherosclerosis. *Eur. J. Prev. Cardiol.* **26**, 15–24 (2019).
11. Gimbrone, M. A. & García-Cardeña, G. Endothelial cell dysfunction and the pathobiology of atherosclerosis. *Circ. Res.* **118**, 620–636 (2016).
12. Jia, G., Aroor, A. R., Jia, C. & Sowers, J. R. Endothelial cell senescence in aging-related vascular dysfunction. *Biochim. Biophys. Acta Mol. Basis Dis.* **1865**, 1802–1809 (2019).
13. Kaur, R., Kaur, M. & Singh, J. Endothelial dysfunction and platelet hyperactivity in type 2 diabetes mellitus: molecular insights and therapeutic strategies. *Cardiovasc. Diabetol.* **17**, 121 (2018).
14. Capsaicin ameliorates intermittent high glucose-. mediated endothelial senescence via the TRPV1/SIRT1 pathway - PubMed. https://pubmed.ncbi.nlm.nih.gov/35405615/
15. Khemais-Benkhiat, S. et al. Angiotensin II-induced redox-sensitive SGLT1 and 2 expression promotes high glucose-induced endothelial cell senescence. *J. Cell. Mol. Med.* **24**, 2109–2122 (2020).
16. Wang, X. et al. Humanin prevents high glucose-induced monocyte adhesion to endothelial cells by targeting KLF2. *Mol. Immunol.* **101**, 245–250 (2018).
17. Donato, A. J., Machin, D. R. & Lesniewski, L. A. Mechanisms of dysfunction in the aging vasculature and role in age-related disease. *Circ. Res.* **123**, 825–848 (2018).
18. The protective effects. Of metformin in an in vitro model of aging 3T3 fibroblast under the high glucose conditions - PubMed. https://pubmed.ncbi.nlm.nih.gov/29512021/
19. Optineurin-mediated mitophagy. Protects renal tubular epithelial cells against accelerated senescence in diabetic nephropathy - PubMed. https://pubmed.ncbi.nlm.nih.gov/29367621/
20. Aguayo-Mazzucato, C. et al. Acceleration of β cell aging determines diabetes and senolysis improves disease outcomes. *Cell. Metab.* **30**, 129–142e4 (2019).
21. Wei, W. & Ji, S. Cellular senescence: Molecular mechanisms and pathogenicity. *J. Cell. Physiol.* **233**, 9121–9135 (2018).
22. Davalli, P., Mitic, T., Caporali, A., Lauriola, A. & D'Arca, D. R. O. S. Cell senescence, and novel molecular mechanisms in aging and age-related diseases. *Oxid Med Cell Longev* 3565127 (2016).
23. Bindokas, V. P. et al. Visualizing superoxide production in normal and diabetic rat islets of Langerhans. *J. Biol. Chem.* **278**, 9796–9801 (2003).
24. Li, X. et al. Exosomes from adipose-derived stem cells overexpressing Nrf2 accelerate cutaneous wound healing by promoting vascularization in a diabetic foot ulcer rat model. *Exp. Mol. Med.* **50**, 1–14 (2018).
25. Li, Y., Jia, Y., Zhou, J. & Huang, K. Effect of methionine sulfoxide reductase B1 silencing on high-glucose-induced apoptosis of human lens epithelial cells. *Life Sci.* **92**, 193–201 (2013).
26. Coradduzza, D. et al. Humanin and its pathophysiological roles in aging: A systematic review. *Biology (Basel)*. **12**, 558 (2023).
27. Mendelsohn, A. R. & Larrick, J. W. Mitochondrial-derived peptides exacerbate senescence. *Rejuvenation Res.* **21**, 369–373 (2018).
28. Xie, Y. et al. Protection effect of [Gly14]-Humanin from apoptosis induced by high glucose in human umbilical vein endothelial cells. *Diabetes Res. Clin. Pract.* **106**, 560–566 (2014).
29. Federici, M. et al. G972R IRS-1 variant impairs insulin regulation of endothelial nitric oxide synthase in cultured human endothelial cells. *Circulation* **109**, 399–405 (2004).
30. Parenti, M. D. et al. Discovery of Novel and selective SIRT6 inhibitors. *J. Med. Chem.* **57**, 4796–4804 (2014).
31. Thompson, C. C. et al. Pancreatic cancer cells overexpress gelsolin family-capping proteins, which contribute to their cell motility. *Gut* **56**, 95–106 (2007).
32. Rodríguez, A. G. et al. Impact of acute high glucose on mitochondrial function in a model of endothelial cells: Role of PDGF-C. *Int. J. Mol. Sci.* **24**, 4394 (2023).
33. Thonsri, U. et al. High glucose-ROS conditions enhance the progression in cholangiocarcinoma via upregulation of MAN2A2 and CHD8. *Cancer Sci.* **112**, 254–264 (2021).
34. Guo, Z. et al. DCAF1 regulates Treg senescence via the ROS axis during immunological aging. *J. Clin. Invest.* **130**, 5893–5908 (2020).
35. Lagnado, A. et al. Neutrophils induce paracrine telomere dysfunction and senescence in ROS-dependent manner. *EMBO J.* **40**, e106048 (2021).
36. Sun, H. J. et al. Polysulfide-mediated sulfhydration of SIRT1 prevents diabetic nephropathy by suppressing phosphorylation and acetylation of p65 NF-κB and STAT3. *Redox Biol.* **38**, 101813 (2021).
37. Xue, Y. et al. Danshensu prevents thrombosis by inhibiting platelet activation via SIRT1/ROS/mtDNA pathways without increasing bleeding risk. *Phytomedicine* **104**, 154271 (2022).
38. Wang, L. et al. Prevalence and treatment of diabetes in China, 2013–2018. *JAMA* **326**, 2498–2506 (2021).
39. Kim, H. J. et al. Association between blood glucose level derived using the oral glucose tolerance test and glycated hemoglobin level. *Korean J. Intern. Med.* **31**, 535–542 (2016).
40. Seo, E., Kang, H., Choi, H., Choi, W. & Jun, H. S. Reactive oxygen species-induced changes in glucose and lipid metabolism contribute to the accumulation of cholesterol in the liver during aging. *Aging Cell.* **18**, e12895 (2019).
41. Rharass, T. & Lucas, S. High glucose level impairs human mature bone marrow adipocyte function through increased ROS production. *Front. Endocrinol. (Lausanne).* **10**, 607 (2019).
42. Stachydrine ameliorates high-. glucose induced endothelial cell senescence and SIRT1 downregulation - PubMed. https://pubmed.ncbi.nlm.nih.gov/23744621/
43. Chen, T. et al. SIRT3 protects endothelial cells from high glucose-induced senescence and dysfunction via the p53 pathway. *Life Sci.* **264**, 118724 (2021).
44. Chi, C. et al. Exerkine fibronectin type-III domain-containing protein 5/irisin-enriched extracellular vesicles delay vascular ageing by increasing SIRT6 stability. *Eur. Heart J.* **43**, 4579–4595 (2022).
45. Pu, Q. et al. Nicotinamide mononucleotide increases cell viability and restores tight junctions in high-glucose-treated human corneal epithelial cells via the SIRT1/Nrf2/HO-1 pathway. *Biomed. Pharmacother.* **147**, 112659 (2022).
46. Kuang, J. et al. The role of Sirt6 in obesity and diabetes. *Front. Physiol.* **9**, 135 (2018).

47. You, Y. & Liang, W. SIRT1 and SIRT6: The role in aging-related diseases. *Biochim. Biophys. Acta Mol. Basis Dis.* **1869**, 166815 (2023).
48. Guo, Z., Li, P., Ge, J. & Li, H. SIRT6 in aging, metabolism, inflammation and cardiovascular diseases. *Aging Dis.* **13**, 1787–1822 (2022).
49. Scisciola, L. et al. New insight in molecular mechanisms regulating SIRT6 expression in diabetes: Hyperglycaemia effects on SIRT6 DNA methylation. *J. Cell. Physiol.* **236**, 4604–4613 (2021).
50. Choe, M. et al. The RUNX2 transcription factor negatively regulates SIRT6 expression to alter glucose metabolism in breast Cancer cells. *J. Cell. Biochem.* **116**, 2210–2226 (2015).
51. Dong, Z. et al. FOXO3a–SIRT6 axis suppresses aerobic glycolysis in melanoma. *Int. J. Oncol.* **56**, 728–742 (2020).
52. Liu, J. et al. CircRNA circ-ITCH improves renal inflammation and fibrosis in streptozotocin-induced diabetic mice by regulating the miR-33a-5p/SIRT6 axis. *Inflamm. Res.* **70**, 835–846 (2021).
53. Niikura, T. Humanin and Alzheimer's disease: The beginning of a new field. *Biochim. Biophys. Acta Gen. Subj.* **1866**, 130024 (2022).
54. Cai, H., Liu, Y., Men, H. & Zheng, Y. Protective mechanism of humanin against oxidative stress in aging-related cardiovascular diseases. *Front. Endocrinol. (Lausanne)*. **12**, 683151 (2021).
55. Boutari, C., Pappas, P. D., Theodoridis, T. D. & Vavilis, D. Humanin and diabetes mellitus: A review of in vitro and in vivo studies. *World J. Diabetes*. **13**, 213–223 (2022).
56. Yen, K. et al. The mitochondrial derived peptide humanin is a regulator of lifespan and healthspan. *Aging (Albany NY)*. **12**, 11185–11199 (2020).
57. Lee, C. et al. The mitochondrial-derived peptide MOTS-c promotes metabolic homeostasis and reduces obesity and insulin resistance. *Cell. Metab.* **21**, 443–454 (2015).
58. Shen, M. Y., Wang, M., Liu, Z., Wang, S. & Xie, Y. [Gly14]-Humanin ameliorates high glucose-induced apoptosis by inhibiting the expression of MicroRNA-155 in endothelial microparticles. *Diabetes Metab. Syndr. Obes.* **14**, 2335–2347 (2021).
59. Zhang, J., Lei, H. & Li, X. The protective effects of S14G-humanin (HNG) against mono-sodium urate (MSU) crystals- induced gouty arthritis. *Bioengineered* **13**, 345–356 (2022).

Author contributions

M.L., Z.L. and X.C. contributed equally. M.L. performed experiments, analyzed the data, and drafted the manuscript, Z.L. designed the experimental validation and analyzed the data. X.C. carried out some supplementary verification of the experimental content. W.X. was responsible for the design of the experimental scheme and the revision of the manuscript. S.W. conducted the extraction and aging staining experiments of primary HUVECs, C.Z. carried out RNA Isolation and Real-Time Quantitative PCR. Y.Z. gave techanical guidance, participated in experimental design and manuscript revision. Y.X. provided constructive discussion about experiments, guided experimental design and manuscript revision. All authors read and approved the final manuscript.

Funding

This work was supported by grants from the National Natural Science Foundation of China [grant number 81670742], Suzhou Municipal Health Bureau [grant number SKJY2021082] and Conversion Base - Endocrinology and Metabolism [grant number ML12301323].

Declarations

Competing interests

The authors declare no competing interests.

Ethics approval

This study was approved by the Ethics Committee of the Second Affiliated Hospital of Soochow University (JD-LK-2022-095-01, July 28, 2022).

Consent to participate

All methods in this study were conducted according to the guidelines and regulations of the Declaration of Helsinki, and all informed consent was obtained from all subjects and/or their legal guardian(s).

Additional information

Supplementary Information The online version contains supplementary material available at https://doi.org/10.1038/s41598-024-81878-x.

Correspondence and requests for materials should be addressed to Y.Z. or Y.X.